IEEE Robotics and Automation Letters (RAL) paper presented at the
2020 IEEE/RSJ International Conference on Intelligent Robots and Systems (IROS)
October 25-29, 2020, Las Vegas, NV, USA (Virtual)

Ultra–thin Joint Torque Sensor with Enhanced Sensitivity for Robotic Application

Dong-Yeop Seok, Yong Bum Kim, Seung Yeon Lee, Jaeyun Kim, and Hyouk Ryeol Choi, *Fellow, IEEE*

***Abstract*— As advanced robotic technologies such as human–robot interaction and automatic assembly processes have emerged, torque sensors have become an essential component for robots. However, commercial torque sensors are not suitable for robotic applications because of their large sizes, heavy weights, narrow options, and high prices. In this letter, we develop a novel capacitive joint torque sensor with ultra-thin structure, high performance, but low cost. To achieve these goals, novel designs have been applied to both the sensing and deformable parts, which are the most important elements of the torque sensor. To obtain high sensitivity, a novel electrode structure called wedge electrode was applied to the sensing part, and a new deformable structure was designed to be ultra-thin and easy to manufacture. Then, the electrode and deformable structures were implemented in a single torque sensor. The developed torque sensor was calibrated based on an artificial neural network (ANN) model and verified to perform high accuracy and sensitivity, and low crosstalk by comparing it with a commercial torque sensor. Finally, a high-performance torque sensor was implemented in ultra-thin size with a diameter of 108 mm and thickness of 13 mm.**

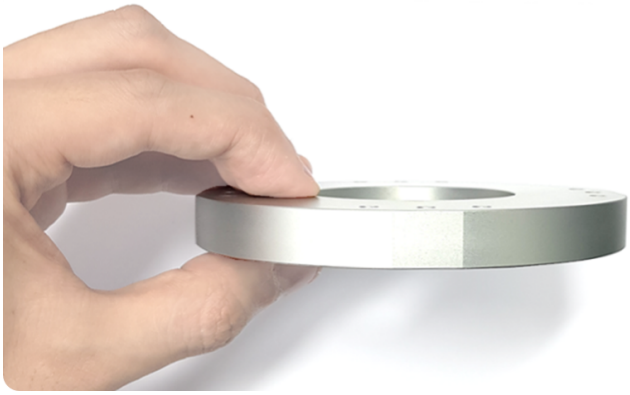

Fig. 1: Ultra-thin capacitive joint torque sensor with finger-thickness.

I. INTRODUCTION

Torque sensors are essential elements for service robots and industrial robots. They improve the reliability and accuracy of a robot, enabling human-robot collaboration, automatic assembly, peg in hole, deburring, and other applications that are not possible with conventional position control [1]-[3]. In particular, torque sensors have recently garnered attention for application in cooperative robots. When users and robots collaborate nearby, unexpected collisions can cause damage to the user. The torque sensor can detect collisions quickly and sensitively, thereby minimizing the damage [4]-[5]. Additionally, because a torque sensor can measure the force exerted by the user, teaching tasks can be performed even with a small force [6].

However, despite the above advantages, commercial torque sensors have not been widely used in robots. This is because commercial torque sensors have large sizes and heavy weights, making the system bulky and heavy when applied. Moreover, they do not offer a wide range of options, and it is thus difficult to find a suitable sensor for robotic applications. And even if there is a suitable sensor, the price is too high, which is a major factor in increasing the overall price of the robot. Most commercial sensors are resistive-type force and torque sensors, and they are manufactured by manually bonding strain gauges. Because of this manual process, these types of sensors are not available for mass production and are expensive to manufacture. Additionally, a signal transducer that amplifies and converts analog signals into digital signals is required outside the sensor to obtain the sensor data. To solve these issues, many resistive-type sensors have been studied [7]-[9]. Kuroki *et al.* developed a highly sensitive, transducer-on-board resistive torque sensor using Cr–N (Nitrogen added Chromium) alloy strain gauges [9]. However, the difficulties of manually bonding multiple strain gauges were not overcome. Other studies also did not solve the inherent problems of the resistance method.

To overcome these limitations, capacitive-type force and torque sensors have been studied [10]-[19]. Kim *et al.* developed a torque sensor by placing two electrodes, that can be simply manufactured without manual processing and have a built-in transducer [10]. However, the structure had low stiffness in the moment direction, making the sensor vulnerable to external forces and moments, causing crosstalk. To solve this problem, a crossed roller bearing was applied [11], though this increased the price of the sensor. Lee *et al.* also developed a capacitive force/torque sensor [12], but the problem was low stiffness and sensitivity. Studies were conducted to improve these two aspects [13]-[14], but the complexity of the sensor structure still represents a manufacturing limit.

In this letter, we have developed a capacitive joint torque sensor with high sensitivity, a low profile structure and low price. Firstly, a new capacitive force sensing method

*This work was supported by the Robot Industry Core Technology Development Program, 20000944, Development of skin type proximity sensing technology for detecting human at 20 cm distance to prevent collision, funded by the Ministry of Trade, Industry and Energy (MI, Korea).

D.-Y. Seok, Y. B. Kim, S. Y. Lee, J. Kim, and H. R. Choi are with the School of Mechanical Engineering, Sungkyunkwan University, Suwon 440- 746, South Korea. dy.seok@skku.edu; yongbum87@me.skku.ac.kr; sylee6051@skku.edu; kjywodbs@skku.edu; choihyoukryeol@gmail.com

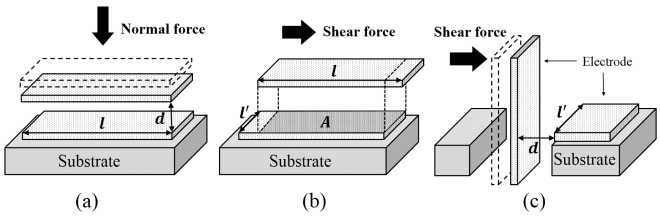

Fig. 2: Conventional capacitive force sensing principles. (a) Capacitance change due to the normal force. (b) Capacitance change due to the shear force. (c) Capacitance between orthogonal electrodes.

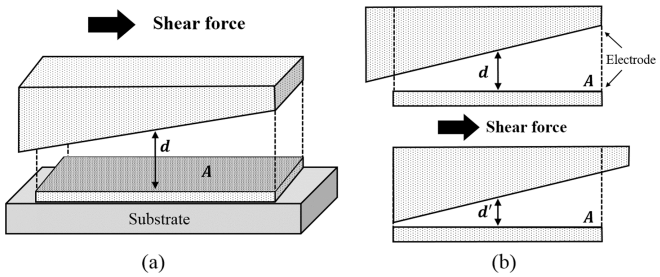

Fig. 3: Wedge electrode structure. (a) A capacitance is formed between inclined electrodes. (b) Shear force is converted into vertical displacement.

is proposed. The proposed electrode structure can measure the torque with more than 2 times higher sensitivity than our previous designs [11], [15] by using an electrode of the inclined structure. Secondly, a new deformable part with a simple and ultra-thin structure is proposed. The proposed structure is very simple to fabricate, reducing greatly the manufacturing cost of the sensor. Finally, both ideas were implemented into an innovative torque sensor. The sensor is an all-in-one sensor including communication circuits and has the thickness of a finger, as shown in Fig. 1. The developed sensor achieves high accuracy and reliability, as verified by applying the ANN-based calibration method and comparing it with commercial torque sensors.

This letter is organized as follows. The new capacitive force sensing method, called wedge electrode, is presented in Section II. In Section III, the new deformable structure is introduced. The implementation of the two designs into a torque sensor is presented in Section IV. Finally, the conclusions are presented in Section V.

II. Electrode design

A. Conventional electrode

A capacitance is formed between the two electrodes. When the external force is applied, the relative position between the two electrodes changes, and the capacitance in turn changes as well. Capacitive-type sensors measure the capacitance difference and calculate the external force and torque [12]. In fact, the capacitance is proportional to the dielectric constant and overlapping area between the electrodes and inversely proportional to their distance. This simple relation is used to produce a change in capacitance. Typically, The change in distance between two parallel electrodes or in the overlapping area produces a change in capacitance as shown in Fig. 2 (a) and (b), respectively. A capacitance change can be expressed as

$$\Delta C = \varepsilon_0 \varepsilon_r \left(\frac{\Delta A}{d_0 - \Delta d} - \frac{\Delta A}{d_0} \right) \tag{1}$$

where ε_0 and ε_r represent the dielectric constant and relative permittivity, respectively. Assuming that $l/d = 10$ in both cases, calculating the change in capacitance when $\Delta d = 0.1 d_0$, with d_0 the initial distance, can be calculated as [15]

$$\begin{aligned} \Delta C_d &= \varepsilon_0 \varepsilon_r 1.1 l' \\ \Delta C_A &= \varepsilon_0 \varepsilon_r 0.1 l' \end{aligned} \tag{2}$$

where ΔC_d and ΔC_A are the capacitance changes due to distance and area change, respectively, and l' represents the width. As a result, the change in capacitance due to the area change is less than 10%. In our previous study, to increase the sensitivity, two electrodes were arranged orthogonally to form a capacitance, as shown in Fig. 2 (c). Even in such arrangement, a high sensitivity was obtained only through fringe effects. In this case, under the same assumptions used in the two previous cases, the change in capacitance is [15]

$$\Delta C_{d_v} = \varepsilon_0 \varepsilon_r 0.47 l' \tag{3}$$

where ΔC_{d_v} is the capacitance change of orthogonal electrodes.

Compared with Equation (2), the amount of change in shear force is increasesd by more than four times. However, the amount of this change is still insufficient, when compared to the normal direction. In torque sensors, because a torque acts as a shear force, the sensitivity in this direction is very important. In particular, one of the most important specifications for torque sensors is the stiffness, which is in a trade-off relationship with sensitivity. Therefore, a large amount of capacitance change is required to satisfy both requirements, and we propose a new electrode structure to achieve this.

B. New wedge electrode

A new electrode structure is developed to achieve higher capacitance change than conventional electrodes. The electrode structure consists of an oblique plane, as shown in Fig. 3 (a), which we named “wedge electrode”. When shear force is applied on this electrode, the movement in the shear direction is transformed into a vertical displacement, as shown in Fig. 3 (b). Thus, the change in shear direction, which has low sensitivity, can be transferred to the normal direction, where the sensitivity is higher. Although this wedge electrode alone can achieve higher sensitivity than that of the existing electrode structures, a composite electrode was developed to obtain even higher sensitivity and capacitance change, as shown in Fig. 4 (a). In this electrode, the left electrode has both an oblique and a vertical plane, and their top, bottom, and side surfaces are the faces of the counter electrode. As shown in Fig. 4 (b), when shear force is applied to this electrode, the capacitance of each component changes, and

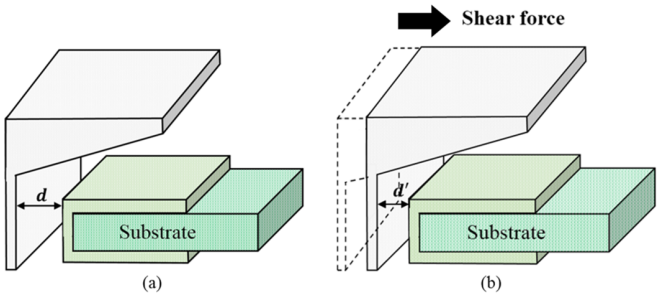

Fig. 4: Capacitive force sensing method with the composite electrode. (a) Structure of composite electrode including wedge electrode. (b) Large capacitance change can be obtained with the electrode structure in shear force.

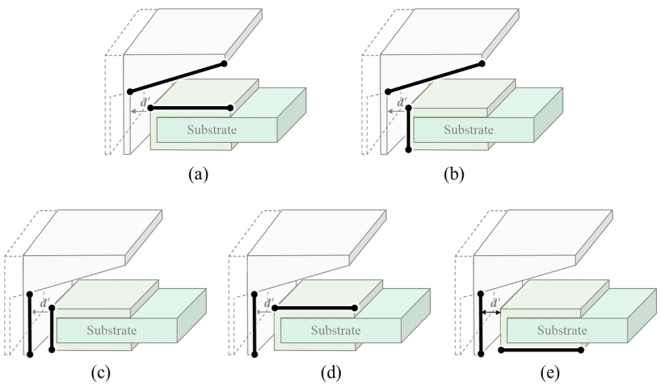

Fig. 5: Capacitance components of the proposed electrode structure. (a) Wedge electrode with a parallel electrode, (b) wedge electode with a vertical electrode, (c) general parallel electrodes, and (d)-(e) perpendicular electrodes.

a very large capacitance difference can be obtained.

The composite electrode has five components, as shown in Fig. 5. The common horizontal and vertical electrodes are formed, and wedge electrodes are formed on both of them. The capacitance of this composite electrode can be derived from the sum of the capacitances of the five elements. First, the wedge capacitance C_{w_h} between the inclined and horizontal electrodes can be derived as [20]

$$\begin{aligned} C_{w_h} &= C_{in} + C_{out} \\ &= \varepsilon_0 \varepsilon_r \left(\frac{K'(k_{in})}{K(k_{in})} + \frac{K'(k_{out})}{K(k_{out})} \right) \end{aligned} \tag{4}$$

where $K(k)$ is the complete elliptic integral of the first kind. k_{in} and k_{out} are the moduli and can be expressed as:

$$k_{in} = \sqrt{\frac{({r_1}^{\pi/\varphi} + {r_2}^{\pi/\varphi})((r_1+l)^{\pi/\varphi} + (r_2+l)^{\pi/\varphi})}{({r_1}^{\pi/\varphi} + (r_2+l)^{\pi/\varphi})({r_2}^{\pi/\varphi} + (r_1+l)^{\pi/\varphi})}} \tag{5}$$

$$k_{out} = \sqrt{\frac{({r_1}^{\pi/2\pi-\varphi} + {r_2}^{\pi/2\pi-\varphi})((r_1+l)^{\pi/2\pi-\varphi} + (r_2+l)^{\pi/2\pi-\varphi})}{({r_1}^{\pi/2\pi-\varphi} + (r_2+l)^{\pi/2\pi-\varphi})({r_2}^{\pi/2\pi-\varphi} + (r_1+l)^{\pi/2\pi-\varphi})}}$$

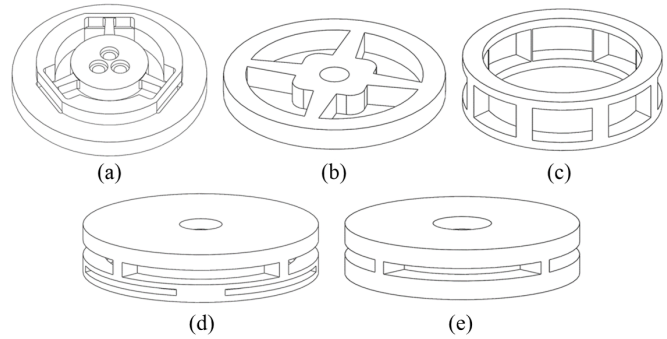

Fig. 6: Conventional deformable structures (a)-(e) typically used for force and torque sensors.

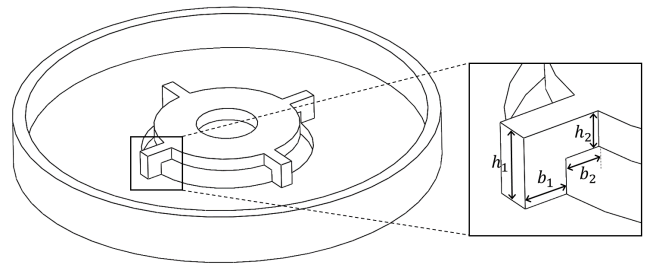

Fig. 7: New deformable structure manufactured by simple machining and design variables for adjusting the responsiveness to 6-axis forces/torques.

where r_1 and r_2 are the distances from the intersection of the extension lines of the two electrodes. φ is angle between two electrodes. Assuming that $r_1 = 0.1l$ and $\varphi = 10°$, the change in capacitance for $\Delta r_2 = 0.1d_0$ can be calculated as

$$\Delta C_{w_h} = \varepsilon_0 \varepsilon_r 0.22 l' \tag{6}$$

Secondly, the wedge capacitance C_{w_v} between the inclined and vertical electrodes can be derived as [21]

$$\begin{aligned} C_{w_v} &= C_{R\,in} + C_{R\,out} + C_{L\,in} + C_{L\,out} \\ &= \varepsilon_0 \varepsilon_r \left(\frac{K'(k_{R\,in})}{K(k_{R\,in})} + \frac{K'(k_{R\,out})}{K(k_{R\,out})} + \frac{K'(k_{L\,in})}{K(k_{L\,in})} + \frac{K'(k_{L\,out})}{K(k_{L\,out})} \right) \end{aligned} \tag{7}$$

where $k_{R\,in}$ and $k_{R\,out}$ are the moduli of the right side, and $k_{L\,in}$ and $k_{L\,out}$ are those of the left side. Because the axes of the two electrodes cross each other, this case can be approximated to the situation of $r_2 = 0$ in Equation (5). Thus, the capacitance change C_{w_v} is

$$\Delta C_{w_v} = \varepsilon_0 \varepsilon_r 0.20 l' \tag{8}$$

The total capacitance change due to the wedge electrode, ΔC_w, is the sum of the two changes above and can be expressed as

$$\Delta C_w = \Delta C_{w_h} + \Delta C_{w_v} = \varepsilon_0 \varepsilon_r 0.42 l' \tag{9}$$

In this way, a shear sensitivity over four times higher than that of sensors that use the area change can be obtained, and the capacitance change is similar to that of the orthogonal

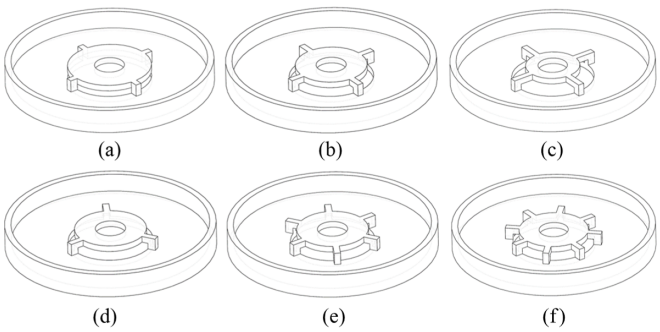

Fig. 8: Various deformable structures (a)-(f) that can be manufactured by adjusting the design variables.

electrode structure. The high-sensitivity composite electrode is developed by combining this wedge electrode and the existing electrode structures. The total capacitance change ΔC_{total} of the composite electrode of Fig. 4 can be expressed as

$$\Delta C_{total} = \Delta C_w + 2\Delta C_{d_v} + \Delta C_d = \varepsilon_0 \varepsilon_r 2.46 l' \qquad (10)$$

which is ten times higher than that reported in our previous study using area change [12], and over five times better than the previous study [15]. Based on the result, a torque sensor with high torque sensitivity can be designed.

III. Structure design

A. Conventional deformable structure

Deformable parts convert external forces into displacements, and they are one of the most important elements in determining the performance and properties of force and torque sensors. However, deformable parts are a major contributor to the price of the sensor because of their complex structure and difficulty in processing and manufacturing. Additionally, there is no optimal structure that can be used from the 1-axis torque sensor to the 6-axis force/torque sensor. In fact, different structures have been commonly used for torque sensors and force/torque sensors.

Representative conventional deformable parts are shown in Fig. 6. Figure 6 (a) and (d) show the structure mainly used for 6-axis force/torque sensors, and (b), (c) and (e) show those mainly used for torque sensors. Thus, one design cannot be applied to all sensors, and it is used limitedly, according to its purpose. Furthermore, structures such as those of Fig. 6 (a) and (c) require special processing such as wire cutting, and those of (d) and (e) require a three-dimensional (3D) machining process, which increases the manufacturing cost of the sensor. Although the structure of (b) is relatively easy to process, its moment stiffness is low, which reduces the performance of the torque sensor.

To solve the problems presented above, we propose a new deformable structure that can be easily processed without special processing and can be designed from torque sensors to 6-axis force and torque sensors in one integrated design.

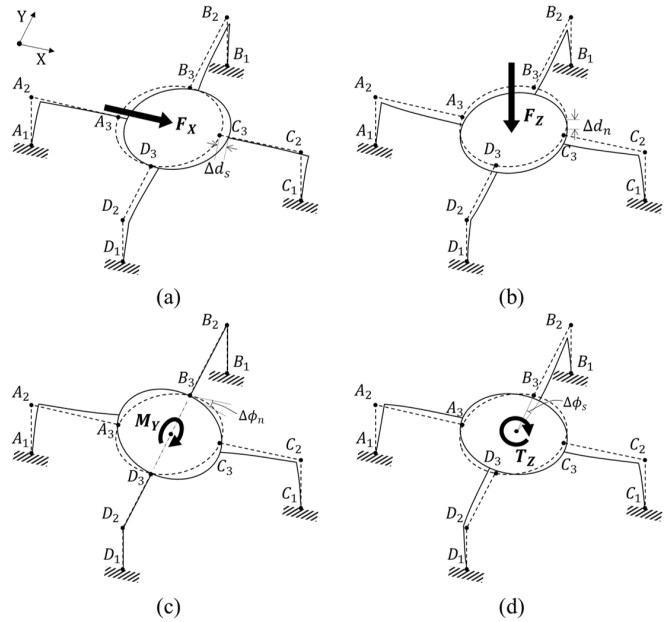

Fig. 9: Mechanical models of the deformable structure composed of four L-shaped beams when the load is (a) F_X, (b) F_Z, (c) M_Y, and (d) T_Z.

B. New deformable structure

The new deformable structure developed is shown in Fig. 7. The developed deformable structure can be manufactured through a simple machining process. By cutting only a part of a hollow cylindrical base, it can be easily fabricated without special processing or 3D machining. Additionally, by adjusting the design variables of the deformable body, it can be extended to various sensor structures. As shown in Fig. 8 (c), all the 6-axis force torques are responsive, so that a 6-axis force/torque sensor structure can also be manufactured. Additionally, because it is fabricated by a simple cutting process, there are no limitations on the number and structure of hinges, as shown in Fig. 8 (d)-(f), so it is possible to manufacture the deformable body which meets the uses and users' needs. In addition to processability and responsiveness and its internal space is used efficiently, allowing a large amount of space in the sensing area. This contributes to the performance of the sensor and enables ultrathin sensor design.

Through a formal analysis of the deformable structure, the 6-axis responsiveness to external forces can be adjusted, and the change in capacitance can be derived. The proposed new deformable structure can be modeled as supported by four similar L-shaped beams, and can be simplified by using the model shown in Fig. 9 when each force or moment and torque is applied. When F_x is applied, as shown in Fig. 9 (a), the displacement of each point can be expressed as [22]

$$\delta_{B_3} = \frac{P_{B_3} {l_1}^3}{3EI} + \frac{P_{B_3} {l_2}^3}{3EI} + \frac{P_{B_3} l_1 {l_2}^2}{JG} \qquad (11)$$

where δ_{B_3} and P_{B_3} are the displacement and load caused by shear force F_X at point B_3, l_1 is length between B_1 and B_2,

and l_2 is length between B_2 and B_3. E, I, J, G represent modulus of elasticity, area moment of inertia, torsional constant, and shear modulus, respectively. At point C_3, shear force F_X causes a displacement and load that can be expressed as

$$\delta_{C_3} = \frac{P_{C_3} {l_1}^3}{3EI} \tag{12}$$

where δ_{C_3} and P_{C_3} are displacement and load at point C_3 by shear force F_X. Structurally, because $\delta_{B_3} = \delta_{C_3} = \Delta d_s$ and $F_X = 2(P_{B_3} + P_{C_3})$, the displacement Δd_s caused by F_X can be expressed as:

$$\Delta d_s = \frac{{l_1}^6 + {l_1}^3 {l_2}^3 + \alpha {l_1}^4 {l_2}^2}{3EI(4{l_1}^3 + 2{l_2}^3 + 2\alpha l_1 {l_2}^2)} F_X \tag{13}$$

where $\alpha = 3EI/JG$. Equation (13) can be used to calculate the displacement of the deformable body caused by shear force F_X(F_Y also structurally symmetrical).

Next, the displacement Δd_n due to normal force F_Z can be expressed as:

$$\Delta d_n = \frac{P_{A_3} {l_2}^3}{3EI} + \frac{P_{A_3} {l_2}^2 l_1}{EI} \tag{14}$$

where P_{A_3} is the load at point A_3 due to normal force F_Z. Structurally, as $P_{A_3} = F_Z/4$, the displacement Δd_n caused by F_Z can be expressed as:

$$\Delta d_n = \frac{1}{4}\left(\frac{{l_2}^3 + 3{l_2}^2 l_1}{3EI}\right) F_Z \tag{15}$$

The angles of rotation caused by moment and torque can be found similar to the displacement. The rotation angle due to moment M_Y(or M_X, structurally symmetrical) can be derived from [22]

$$\phi_{r_n} = \frac{T_{r_n} l_2}{JG} \tag{16}$$

where ϕ_{r_n} is the rotation angle caused by moment M_Y and T_{r_n} is the loaded torque at P_{B_3} or P_{D_3} due to M_Y. And in the same situation, the vertical displacement $delta_{r_n}$ of P_{C_3} can be expressed as

$$\delta_{r_n} = \frac{P_{r_n} {l_2}^3}{3EI} + \frac{P_{r_n} {l_2}^2 l_1}{EI} \tag{17}$$

where P_{r_n} is the equivalent load due to moment M_Y at point P_{C_3}. Structurally, $\delta_{r_n} = r\phi_{r_n}$ and $M_Y = 2(T_{r_n} + rP_{r_n})$ where r is the radius of the circular plate of Fig. 9. Then the rotation angle ϕ_{r_n} due to M_Y is expressed as

$$\phi_{r_n} = \frac{{l_2}^4 + 3{l_2}^3 l_1}{2JG({l_2}^3 + 3{l_2}^2 l_1 + \alpha r^2 l_2)} M_Y \tag{18}$$

Finally, the rotation angle due to torque can also be derived through the deformation and structural relationship at each point. Displacement $delta_{r_s}$ caused by the torque T_Z at point P_{B_3} can be expressed as:

$$\delta_{r_s} = \frac{P_{r_s} {l_1}^3}{3EI} + \frac{P_{r_s} {l_2}^3}{3EI} + \frac{P_{r_s} l_1 {l_2}^2}{JG} \tag{19}$$

where P_{r_s} is the equivalent load caused by torque T_Z at point P_{B_3}. Structurally, $T_Z = 4rP_{r_s}$ and the rotation angle ϕ_{r_s} caused by torque T_Z is calculated as

$$\phi_{r_s} = \frac{1}{4r^2}\left(\frac{{l_1}^3 + {l_2}^3}{3EI} + \frac{l_1 {l_2}^2}{JG}\right) T_Z \tag{20}$$

Even if the number of L-shaped beams changes, the displacement and rotation angle can be calculated with the above procedure.

In conclusion, the displacement caused by an external force loaded on the sensor can be obtained from Equations (13), (15), (18), and (20). Thus, it is possible to design a sensor with the desired sensing range by adjusting the relevant variables. Furthermore, the capacitance change due to the external forces and torques can be calculated using Equations (1) and (10).

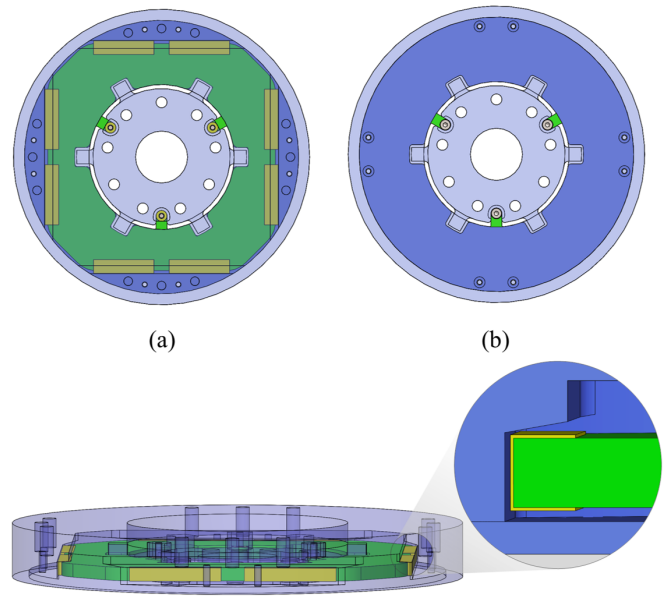

Fig. 10: Structure of the developed torque sensor: (a) top view, (b) bottom view, and (c) side-perspective view, with composite electrodes including the wedge electrode formed inside.

IV. Implementation into Sensor

A. Implementation

The wedge electrode structure and the new deformable structure are implemented in a single torque sensor. The structure of the sensor is shown in Fig. 10. The deformable structure is designed based on the above mentioned formula analysis and is robust not only in the torque direction but also in the moment direction and against forces in each axis. A sensing printed circuit board (PCB) is placed in the empty space inside the deformable structure. As shown in Fig. 10 (a), eight electrodes were placed on the edge of the sensing PCB. As shown in Fig. 10 (c), the inner periphery of the deformable structure is designed as the proposed composite electrode. The deformable structure is electrically grounded to form a capacitance with the electrodes of the sensing PCB.

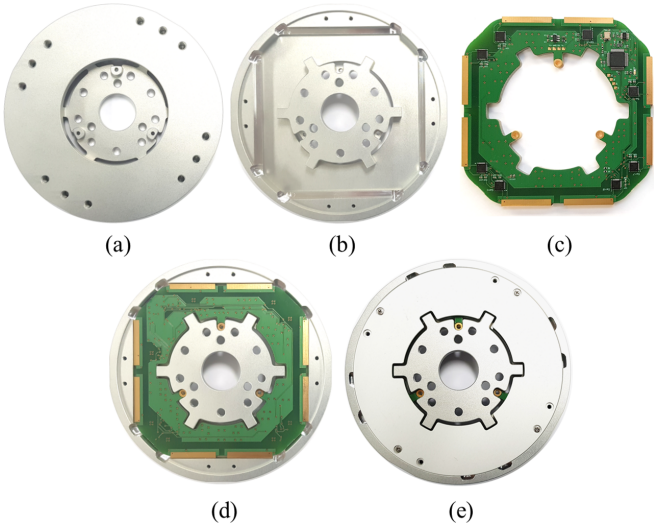

Fig. 11: Structure and assembly process of developed torque sensor. (a) Frontside and (b) backside of the fabricated deformable structure, and (c) the sensing PCB. (d)-(e) show assembly process.

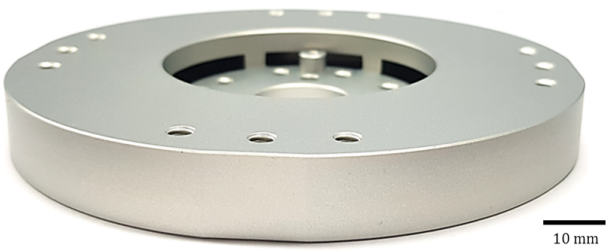

Fig. 12: Fully assembled view of the developed joint torque sensor.

That is, capacitances are formed between eight electrode pairs, and the change of the corresponding eight capacitances can measure all six-axis force and torque elements. Using this, it is possible to obtain an accurate measurement of the torque, decoupled from all the forces and moments on other axes. Finally, a cover is designed on the backside of the sensor to block noise from the outside and prevent the entrance of foreign matter.

B. Fabrication

The torque sensor was fabricated based on the designed electrodes and deformable structure. In manufacturing the torque sensor, to reduce the manufacturing cost and allow mass production, the manufacturability and assembly were considered.

The deformable structure can be processed by simple two-dimensional (2D) machining, and casting is also possible, which can improve mass productivity and reduce cost. The inner electrode surface can also be processed at once through simple machining. The sensing PCB includes the electrodes,

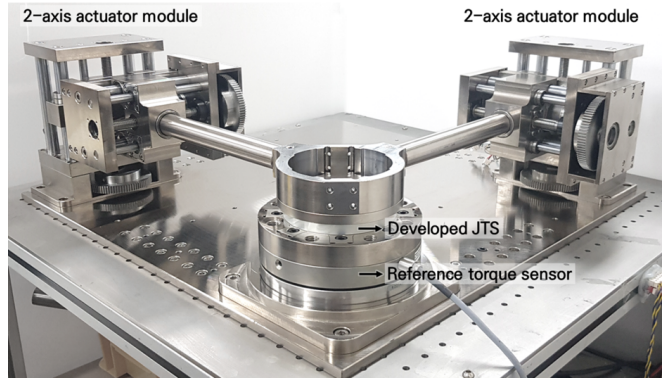

Fig. 13: Torque sensor calibration setup with two 2-axis actuator modules and reference torque sensor.

capacitance digital convertor (CDC) chips (AD7147, Analog Devices) that measure and convert the capacitance to digital values, ARM processors (STM32F103, ST), and CAN communication chips. Thus, no additional equipment is required for torque measurement, and the sensor thus fabricated is robust against disturbances because it outputs a digital signal.

The assembly process of the sensor is also very simple. First, the PCB is introduced into the deformable structure and fixed with bolts, as shown in Fig. 11 (d). To block external influences such as electromagnetic waves, the sensor is covered and bolted as shown in Fig. 11 (e). Because there is no manual process and the manufacturing is simple, this sensor can be fabricated at a price less than 1/30 of that of a commercial torque sensor. Aluminum 7075-t6 was selected as the main material of the sensor to reduce its weight and satisfy the rigidity requirements. Additionally, anodization was applied to shield the sensor electrically from the outside.

The completed joint torque sensor is shown in Fig. 12. The torque sensor is ultra-thin with a diameter of 108 mm and thickness of 13mm, and its rated torque is 200Nm. The mechanical specifications of the developed torque sensor are reported in Table 1.

TABLE I: SPECIFICATIONS OF THE DEVELOPED TORQUE SENSOR

Property	Value	Unit
Dimension	ϕ 108 x H 13	mm
Weight	210	g
Nominal torque	$\pm$ 200	Nm
Peak torque	$\pm$ 350	Nm
Load capacity	F_{xyz}: $\pm$ 2000, M_{xy}: $\pm$ 200	N, Nm
Stiffness	Torque:1.5×10^5, Moment:1.1×10^5	Nm/rad
Communication	CAN	-
Frequency	1,000	Hz

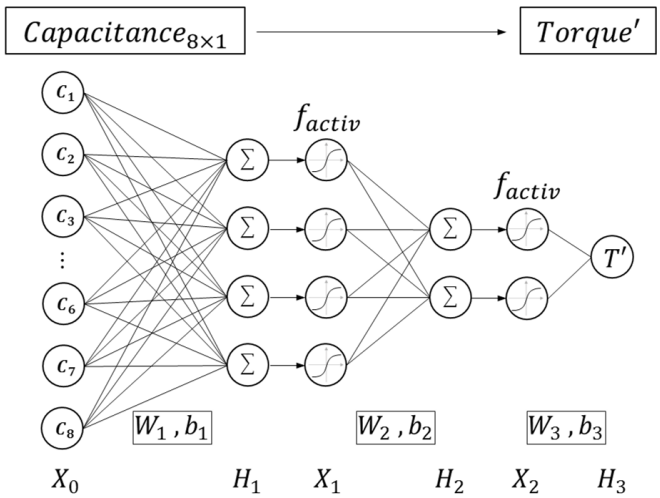

Fig. 14: Artificial neural network (ANN) model applied to the torque sensor calibration.

V. Calibration and Evaluation

A. Calibration

Because the fabricated sensor measures the capacitance, this has to be converted into a force or torque through a calibration process. In our previous studies, we used linear combinations [11] and nonlinear fits [15] for the calibration, though the results have been unsatisfactory in terms of accuracy and decoupling. It was also difficult to obtain high-quality calibration data sets by manually applying force and torque during calibration, and it was impossible to apply high loads.

In this letter, an artificial neural network (ANN) model is applied to the calibration to achieve high performance. A calibration unit was developed and used to collect high-quality training data sets and automate calibration, as shown in Fig. 13. The calibration jig has two-axis actuator modules attached to each lever to apply a combination of forces, moments, and torques to the sensor. The developed sensor and a reference commercial torque sensor (TB1A, HBM) were fixed to load the same forces and torques. The ANN model, shown in Fig. 14, consists of an input layer, two hidden layers, and an output layer. The input layer consists of eight nodes, where the input is the normalized capacitance measured at the eight electrodes. The two hidden layers consist of four and two nodes, respectively, and use a logistic sigmoid function as the activation function. Finally, the normalized torque is the output at the output layer. The calculations for each layer can be expressed as

$$H_n = W_n {X_{n-1}}^T + b_n \tag{21}$$

$$X_n = f_{activ}(H_n) = \frac{1}{1+e^{-H_n}} \tag{22}$$

where W_n and b_n are the weight and bias, respectively, and f_{activ} is the activation function. Finally, the torque value can be obtained by denormalizing H_3 as follows:

$$Torque\ [Nm] = \frac{(T_{max} - T_{min})(H_3 + 1)}{2} + T_{min} \tag{23}$$

where T_{max} and T_{min} are the maximum and minimum torque. A simple ANN structure of 3-layer was adopted and trained by MATLAB. All the above calculations are embedded in the ARM processor inside the torque sensor, which outputs the final torque value calculated.

Through the above calibration jig and ANN model, torque sensor with built-in calibration, high accuracy, and decoupling performance was manufactured.

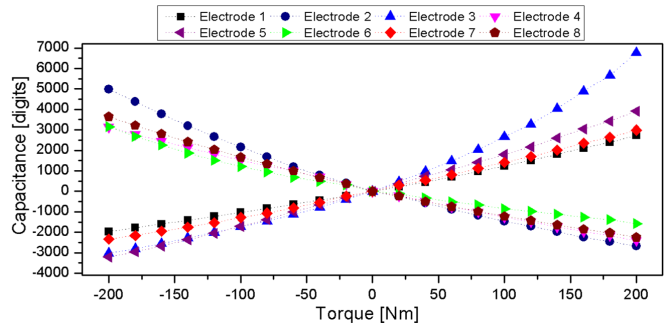

Fig. 15: Capacitance changes of the 8-electrode cells according to the loaded torque.

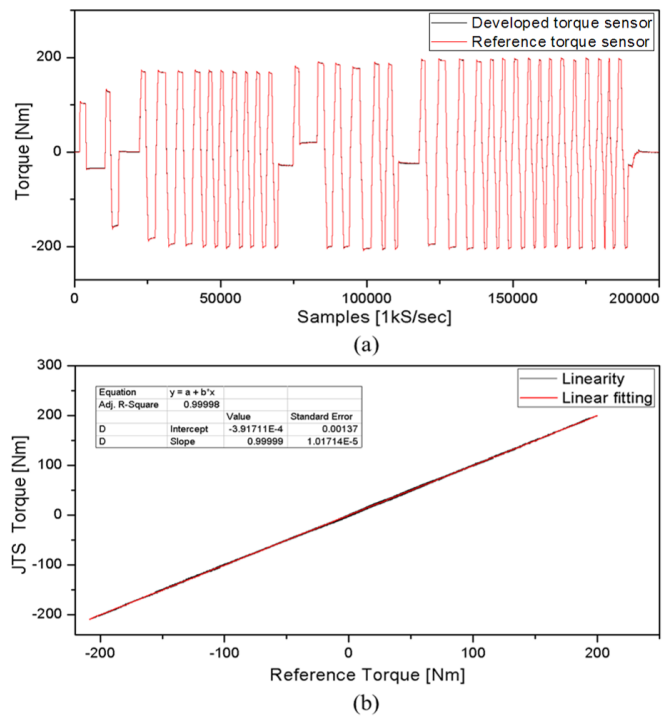

Fig. 16: Experimental results of developed torque sensor. (a) Comparison of torques measured by the developed torque sensor (black) and the reference sensor (red). (b) Linearity plot.

B. Evaluation

When torque is applied to the developed torque sensor, the variation of each cell according to torque is shown in

TABLE II: PERFORMANCE OF THE SENSOR

Property	Value	Unit
Accuracy	99.88	%
Linearity	99.83	%
Repeatability	99.77	%
Hysteresis	≤ 0.3	%
Torque resolution*	0.12	Nm

*The torque resolution is calculated as the standard deviation of the sample.

Fig. 15. The average capacitance change in the cells was approximately 6300 digits from the CDC, which is several times higher than that of previous studies. Because the air gap between the electrodes was set to 150 um in the developed sensor to facilitate its assembly, the sensitivity can be considered to be 10 times higher than that of previous studies [10]-[12].

To verify the performance of the fabricated torque sensor, its measurements were compared with those of the commercial torque sensor. As shown in Fig. 16 (a), the values of the two sensors are perfectly matched. In this test, a combination of torques, forces, and moments was applied to the sensors, with values of $\pm$200 Nm, $\pm$1 kN, and $\pm$150 Nm, respectively. Nevertheless, the value of the torque was accurate and perfectly decoupled, as that of the reference sensor. Additionally, a very high linearity was confirmed, as shown in Fig. 16 (b). The performance of the developed torque sensor (accuracy, linearity, etc.) is reported in Table 2. As seen, the developed sensor achieves a performance comparable to that of commercial sensors.

VI. CONCLUSIONS

In this letter, a novel capacitive joint torque sensor with a wedge electrode and ultra-thin structure is presented. First, a new capacitive force sensing method was proposed using wedge electrodes with inclined shape. Further, a new composite electrode structure including the wedge electrodes was developed to obtain a large capacitance variation. Second, a new deformable structure that is easy to process and allows manufacturing of ultra-thin sensors was proposed. The deformable structure makes it easy to adjust the responsiveness of the sensor to 6-axis forces and torques and can be used as an integrated design for all sensors.Finally, the wedge electrode structure and the new deformable structure were implemented in a single torque sensor. An ANN-based calibration model was applied to the fabricated sensor and compared with a reference sensor. From the comparison, the performance of the developed torque sensor was comparable to those of commercial torque sensors.

In conclusion, a high-performance, ultra-thin, lightweight, easy-to-machine and -assemble, low-cost, and innovative torque sensor has been developed. The sensor is expected to be widely applicable to robotic systems.

REFERENCES

[1] C. Ott, A. Albu-Schaffer, A. Kugi, and G. Hirzinger, "On the Passivity-Based Impedance Control of Flexible Joint Robots," *IEEE Trans. on Robot.*, vol. 24, no. 2, pp. 416–429, 2008.

[2] W. Bluethmann, R. Ambrose, M. Diftler, S. Askew, E. Huber, M. Goza, F. Rehnmark, C. Lovchik, and D. Magruder, "Robonaut: A robot designed to work with humans in space," *Auton. Robots*, vol. 14, pp. 179–197, 2003.

[3] A. Bicchi and G. Tonietti, "Fast and soft arm tactics: Dealing with the safety-performance trade-off in robot arms design and control," *IEEE Robotics and Automation Mag.*, vol. 11, pp. 22–33, 2004.

[4] S. Haddadin, A. D. Luca, and A. Albu-Schaffer, "Robot Collisions: A Survey on Detection, Isolation, and Identification," *IEEE Trans. Robot.*, vol. 33, no. 6, pp. 1292–1312, 2017.

[5] A. D. Luca, A. Albu-Schaffer, S. Haddadin, and D. Hirzinger, "Collision Detection and Safe Reaction with the DLR-III Lightweight Manipulator Arm," in *Proc. IEEE/RSJ Int. Conf. Intell. Robot. Syst.*, 2006, pp. 1623–1630.

[6] Y. Kim, K. Ahn, and J. Song, "Direct teaching algorithm based on task assistance for machine tending," in *Proc. IEEE Int. Conf. Ubiquitous Robot. Ambient Intell.*, 2016, pp. 861–866.

[7] S. Lee, K. Yang, E. Shin, and H. Kim, "Development of 1-axis torque sensor with different shape of support and measurement spoke," in *Proc. IEEE Int. Conf. Ubiquitous Robot. Ambient Intell.*, 2014, pp. 688–691.

[8] C. Yuan, L. -P. Luo, Q. Yuan, J. Wu, R. -J. Yan, H. Kim, K. -S. Shin, and C. -S. Han, "Development and evaluation of a compact 6-axis force/moment sensor with a serial structure for the humanoid robot foot," *Measurement*, vol. 70, pp. 110–122, 2015.

[9] Y. Kuroki, Y. Kosaka, T. Takahashi, E. Niwa, H. Kaminaga, and Y. Nakamura, "Cr-N Alloy Thin-film Based Torque Sensors and Joint Torque Servo Systems for Compliant Robot Control," in *Proc. IEEE Int. Conf. Robot. Autom.*, 2013, pp. 4954–4959.

[10] Y. B. Kim, U. Kim, D. -Y. Seok, J. So, and H. R. Choi, "A novel capacitive type torque sensor for robotic applications," in *Proc. IEEE Int. Conf. Advanced Intelligent Mech.*, 2016, pp. 993–998.

[11] Y. B. Kim, U. Kim, D. -Y. Seok, J. So, Y. H. Lee, and H. R. Choi, "Torque Sensor Embedded Actuator Module for Robotic Applications," *IEEE/ASME Trans. Mech.*, vol. 2, no. 4, pp. 1662–1672, 2018.

[12] D.-H. Lee, U. Kim, H. Jung, and H. R. Choi, "A Capacitive Type Novel 6-Axis Force/Torque Sensor for Robotic Applications," *IEEE Sens. J.*, vol. 16, pp. 2290–2299, 2016.

[13] J. -I. Kim, H. -S. Jeon, Y. -J. Jeong, and Y. -J. Kim, "High Stiffness Capacitive Type Torque Sensor with Flexure Structure for Cooperative Industrial Robots," in *Proc. IEEE Int. Conf. Ubiquitous Robot. Ambient Intell.*, 2017, pp. 433–437.

[14] Y. Yu, T. Chaen, and S. Tsujio, "High-Stiffness and High-Sensitivity 3-Axis Force Sensor Using Strain-Deformation Expansion Mechanism," in *Proc. IEEE/RSJ Int. Conf. Intell. Robot. Syst.*, 2006, pp. 4417–4422.

[15] U. Kim, D.-H. Lee, Y. B. Kim, D.-Y. Seok, and H. R. Choi, "A novel six-axis force/torque sensor for robotic applications," *IEEE/ASME Trans. Mech.*, vol. 22, no. 3, pp. 1381–1390, 2017.

[16] U. Kim, Y. B. Kim, J. So, D. -Y. Seok, and H. R. Choi, "Sensorized Surgical Forceps for Robotic-Assisted Minimally Invasive Surgery", *IEEE Trans. Ind. Electron.*, vol. 65, pp. 9604–9613, 2018.

[17] D.-Y. Seok, Y. B. Kim, U. Kim, S. Y. Lee, and H. R. Choi, "Compensation of environmental influences on sensorized-forceps for practical surgical tasks," *IEEE Robot. Autom. Lett.*, vol. 4, no. 2, pp. 2031–2037, 2019.

[18] U. Kim, D.-H. Lee, W. J. Yoon, B. Hannaford, and H. R. Choi, "Force Sensor Integrated Surgical Forceps for Minimally Invasive Robotic Surgery," *IEEE Trans. Robot.*, vol. 31, no. 5, pp. 1214-1224, 2015.

[19] U. Kim, Y. B. Kim, D.-Y. Seok, J. So, and H. R. Choi, "A Surgical Palpation Probe with 6-Axis Force/Torque Sensing Capability for Minimally Invasive Surgery," *IEEE Trans. Ind. Electron.*, vol. 65, no. 3, pp. 2755–2765, 2018.

[20] Y. Xiang, "The electrostatic capacitance of an inclined plate capacitor," *J. Electrostat.*, vol. 64, pp. 29–34, 2006.

[21] Y. Xiang, "Further study on electrostatic capacitance of an inclined plate capacitor," *J. Electrostat.*, vol. 66, pp. 366–368, 2008.

[22] A.C. Ugural and S.K. Fenster, *Advanced strength and applied elasticity*, 4th ed. Englewood Cliffs, NJ: Prentice Hall, 2003.